International Journal of Mining Science and Technology 30 (2020) 623–633

Contents lists available at ScienceDirect

International Journal of Mining Science and Technology

journal homepage: www.elsevier.com/locate/ijmst

Numerical simulation on borehole breakout and borehole size effect using discrete element method

H. Lin [a], W.H. Kang [b], J. Oh [a,*], I. Canbulat [a], B. Hebblewhite [a]

[a] School of Minerals and Energy Resources Engineering, University of New South Wales, Sydney, NSW 2052, Australia
[b] Centre for Infrastructure Engineering, Western Sydney University, Penrith, NSW 2751, Australia

ARTICLE INFO

Article history:
Received 11 January 2020
Received in revised form 5 April 2020
Accepted 24 May 2020
Available online 30 May 2020

Keywords:
Borehole breakout
Breakout angular span
Borehole size effect
Numerical simulation
Thermal effect

ABSTRACT

Estimation of horizontal stress magnitudes from borehole breakouts has been an attractive topic in the petroleum and mining industries, although there are critical research gaps that remain unfilled. In this paper, numerical simulation is conducted on Gosford sandstone to investigate the borehole breakout and its associated borehole size effect, including temperature influence. The discrete element method (DEM) model shows that the borehole breakout angular span is constant after the initial formation, whereas its depth propagates along the minimum horizontal stress direction. This indicates that the breakout angular span is a reliable parameter for horizontal stress estimation. The borehole size effect simulations illustrated the importance of borehole size on breakout geometries in which smaller borehole size leads to higher breakout initiation stress as well as the stress re-distribution from borehole wall outwards through micro-cracking. This implies that the stress may be averaged over a distance around the borehole and breakout initiation occurs at the borehole wall rather than some distance into the rock. In addition, the numerical simulation incorporated the thermal effect which is widely encountered in deep geothermal wells. Based on the results, the higher temperature led to lower breakout initiation stress with same borehole size, and more proportion of shear cracks was generated under higher temperature. This indicates that the temperature might contribute to the micro-fracturing mode and hence influences the horizontal stress estimation results from borehole breakout geometries. Numerical simulation showed that breakout shape and dimensions changed considerably under high stress and high temperature conditions, suggesting that the temperature may need to be considered for breakout stress analysis in deep locations.

1. Introduction

A borehole breakout occurs during the drilling process in mining and oil operations or circular underground excavation including tunneling [1–4]. In general, the "dog-ear" shaped breakout is the most commonly encountered breakout type in the field and is widely used in horizontal stress orientation indication as the "dog-ear" tip is well aligned with the minimum horizontal principal stress (σ_h) direction [4–9]. To date, due to increasing resource exploitation depth and the rapid advancement of downhole logging technology, breakout geometries illustrated in Fig. 1 have been used extensively in horizontal stress magnitude estimation and constraint, especially via the breakout angular span (θ_b) [2,6,7,10–12]. However, the explicit relationship between the breakout geometries and the horizontal principal stresses remains unclear.

To study the relationship and understand the mechanism of breakout formation, a series of researchers have performed laboratory breakout studies on various rock types, including sandstone and limestone [13–20]. Based on the experimental findings, it is observed that both breakout geometries are sensitive to the change of horizontal principal stress magnitudes [16,19–21]. The resultant borehole breakout is wider and deeper under higher maximum horizontal principal stress (σ_H) while the minimum horizontal and vertical principal stress (σ_v) are constant; and the rate of breakout geometry expansion tends to increase with the magnitudes of σ_h and σ_v with the same horizontal stress ratio applied [16,17,20]. Some researchers have also argued that there is a unique relationship between the two geometries regardless of stress conditions, so that the two geometries are redundant parameters for horizontal stress estimation [16,19,21–23]. In addition, many studies suggested that θ_b is a more reliable parameter than

* Corresponding author.
E-mail address: joung.oh@unsw.edu.au (J. Oh).

https://doi.org/10.1016/j.ijmst.2020.05.019
2095-2686/

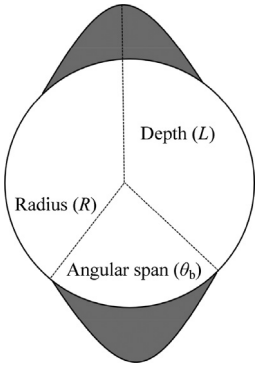

Fig. 1. Breakout geometries (after [46]).

Fig. 2. UNSW confinement cell (after [46]).

the normalised breakout depth (L/R) as it forms quickly at an early stage of the breakout and is followed by the subsequent development of breakout depth without any further widening [6,20,24–29].

As mineral resources at shallow depths are quickly extracted to meet the increasing global demand, exploration and exploitation activities at deeper locations have gained considerable attention. For instance, the current geothermal well has been carried out up to 5000 m depth [30], and mining operations in many countries occur at more than 1000 m depth, including South Africa, China and Ukraine [31–35]. In deep locations, the temperature is usually high and can have impact on the mechanical properties of rock [36]. This thermal effect may also influence the breakout geometries and thus disturb the horizontal stress estimation. Due to limitations in laboratory conditions, it is difficult to perform true triaxial tests on samples under various temperatures.

Numerical analysis is a powerful tool which can simulate different scenarios, including the high temperature [37–39]. Many researchers have implemented the numerical technique to study the formation mechanism and geometries of borehole breakout under different stress conditions [20,24,39–45]. This paper first discusses the breakout experimental results from Gosford sandstone, and then investigates the detailed parametric study on borehole breakout and borehole size, including horizontal stress conditions, borehole size as well as the thermal effect via the discrete element method (DEM) software PFC2D. Results of this study will develop a more clear understanding of breakout geometrical development throughout the process and the micro-cracking mode; thereby, identifying critical parameters for horizontal stress estimation from borehole breakout.

2. Experimental data

Existing experimental data was used in this study to validate the numerical simulation results. Cubic Gosford sandstone samples ($120 \times 120 \times 120$ mm^3) with pre-drilled holes (8, 11 and 15 mm radii) were loaded under true triaxial stress conditions ($\sigma_H > \sigma_h > \sigma_v$) using a specially designed confinement cell (Fig. 2) at room temperature to mimic field scenarios. The experiments applied various maximum horizontal principal stresses while keeping the minimum horizontal and vertical principal stress magnitudes at the same level. At the completion of experiments, samples were cut in half along the maximum horizontal principal stress direction and underwent the optical scanning to precisely measure the breakout geometries. A detailed description of the experimental procedures is given in Lin et al. [46].

The interpretation of experimental results suggests that both breakout geometries are dependent on the maximum horizontal principal stress magnitudes in which the higher maximum horizontal principal stress led to wider and longer breakouts (see Fig. 3). Results showed an overall agreement with previous researches [16,19,21,47], indicating there is a definite relationship between breakout geometries and horizontal stress magnitudes. It can also be seen that the larger hole size resulted in wider and deeper breakouts under the same stress conditions. This is also in line with the observations from Haimson & Herrick [14], Carter [48] and Bažant et al. [49], where the stress required to initiate borehole breakout is much higher for the smaller borehole size than that of the larger ones. In addition, the angular expansion and deepening rate of breakouts with 8 and 11 mm borehole radii appear steady and similar with increasing maximum horizontal stress, whereas the rate at 15 mm borehole radius is much higher.

3. Numerical simulation

3.1. Particle flow code

Although breakout geometries under different stress conditions were investigated in the laboratory, the formation mechanism cannot be effectively studied due to the limitation of the equipment. It is not possible to capture the breakout geometries at various stages of the experiment unless the sample is taken out of the equipment for CT-scanning numerous times during the test. To overcome the shortcomings of the experimental work and study the breakout geometries in detail, two-dimensional particle flow code (PFC2D) was implemented in this study to reproduce the laboratory results. PFC2D is software developed by Itasca Group using the DEM in which the rock is represented by an assembly of solid particles that are bonded by the cementing material in between [50]. Cracking occurs at the contact bonds if the associated tensile or shear force exceeds the corresponding strengths, while the coalescence of bond breakages can represent the macro-fracture initiation and development. The governing fracture criterion is Mohr Coulomb.

In general, there are two types of basic bond model i.e. the contact bond (CB) and parallel bond (PB) models. The CB model is considered as a "point of contact" between particles whereas the PB model is envisioned as a beam distributed along a rectangular area and centered at the point of contact. In recent years, flat-joint model has also gained significant attention in simulating the rock behavior [51,52]. In this study, the PB model was adopted to closely simulate the breakout phenomenon; this is primarily due to its popularity in previous numerical investigation on borehole related studies [20,24,53–56].

3.2. Model calibration

In PFC2D, the physical properties cannot be directly assigned to the synthetic sample and a "trial and error" process is required to

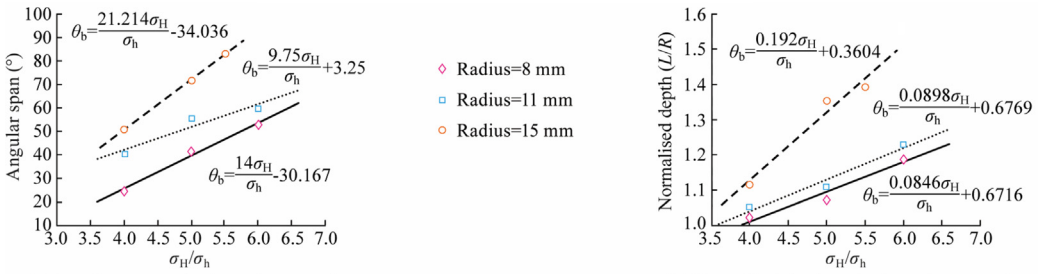

(a) Angular span vs. horizontal stress ratio

(b) Normalised depth vs. horizontal stress ratio

Fig. 3. Breakout geometries vs. horizontal stress ratio (after [46]).

calibrate the micro-mechanical properties of synthetic rock against the macro-responses of Gosford sandstone. For this purpose, a 42 × 100 mm^2 specimen was generated in the model with the particle radius ranging from 0.20 to 0.28 mm. Based on the calibration methodology proposed by Potyondy & Cundall [57], the uniaxial compressive strength (UCS), Young's modulus (E) and Poisson's ratio (υ) of the synthetic rock were matched against the laboratory results. Correspondingly, the appropriate micro-mechanical properties of the particles and parallel bonds were determined [58,59], as summarized in Table 1. Table 2 shows the macro-mechanical properties of both synthetic and experimental rock samples, which indicate that the synthetic specimen was properly calibrated.

3.3. Simulation procedures

Based on the calibration results, a rock specimen with dimensions of 120 × 120 mm^2 was generated with the micro-properties listed in Table 1, which consists of a total of 70,930 particles. In the laboratory conditions, boreholes (8, 11, and 15 mm radii) were drilled prior to the loading phase. To closely simulate the experiment, holes were also created in the center of the sample before applying stresses. Fig. 4 illustrates the specimen setup and loading directions.

In the model, horizontal stresses were applied by moving the platens inwards, governed by a servo-control mechanism. The mechanism auto-corrects the applied stresses by adjusting the velocities of boundary walls so that the pre-set stresses can be reached and maintained throughout the test [50]. Initially, both σ_H and σ_h were increased simultaneously until 10 MPa. By then, σ_h was kept at the same level while increasing σ_H to the target value to allow the development of borehole breakout.

Fig. 5 shows a simulation result of borehole breakout with 11 mm borehole radius, where σ_H = 50 MPa and σ_h = 10 MPa. The breakout tip is sub-parallel to the lateral direction, showing that the borehole breakout depth is in line with the minimum horizontal principal stress direction. This suggests that the breakout depth can be used as a reliable indicator of the horizontal stress orientation, which has been used extensively in field studies [4,5,10,25,60,61]. The contact between particles can be broken by either shear or tensile failure, as shown by the red and black dashes in the vicinity of the borehole in Fig. 5. Fig. 5 shows the majority of micro-cracks were formed in tensile failure whereas only a few were formed due to shear failure [20,24]. As the micro-cracks coalesce and intersect with each other, a "dog-ear" shaped breakout was created, which is consistent with Fig. 1.

Table 1
Micro-mechanical properties of particles and bonds.

Particle micro-mechanical property		Parallel bond micro-mechanical property	
Density (kg/m^3)	2650	Young's modulus (GPa)	3
Young's modulus (GPa)	3	Normal strength (MPa)	27 ± 6
Coefficient of friction (MPa)	0.58	Shear strength (MPa)	27 ± 6
Stiffness ratio (k_n/k_s)	1.5	Stiffness ratio (k_n/k_s)	1.5

Table 2
Physical and numerical rock properties.

Parameter	Experimental	Numerical
UCS (MPa)	42.3	43.0
Young's modulus (GPa)	7.5	7.54
Poisson's ratio	0.18	0.182

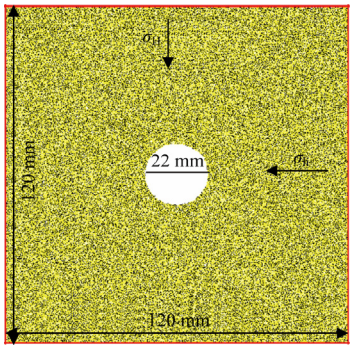

Fig. 4. Illustration of the numerical simulation.

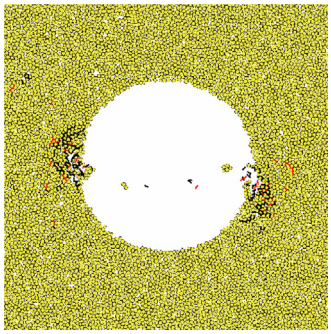

Fig. 5. Borehole breakout simulated under σ_H = 50 MPa and σ_h = 10 MPa with 11 mm radius, where tensile failure is represented by the black dash and the shear failure is represented by the red dash.

4. Simulation results and discussion

4.1. Borehole breakout under various horizontal stress magnitudes

A series of numerical simulations were carried out on synthetic Gosford sandstone to study the behavior of borehole breakout.

Fig. 6a–f illustrate the breakout development of a 15 mm radius borehole under σ_H = 50 MPa and σ_h = 10 MPa. As shown in Fig. 6a and b, breakout initially formed as rock slabs which are sub-parallel to the direction of maximum horizontal principal stress and subsequently spalled off towards the center of the borehole, indicated by the movement of detached particles. By then, a fracture plane formed along the borehole breakout propagation direction from the maximum point of the fracture at the borehole wall to the breakout tip (see Fig. 6c and d). Eventually, fractures were localised at the tip of the breakout and induced minor breakout propagation due to the stress re-distribution and concentration from the failure zone, as shown in Fig. 6e and f. The progress of breakout development followed the same pattern as discussed by Cuss et al. [18] from their experimental observations on Tennessee sandstone. Numerical results imply that breakout is caused by the combination of shear and tensile failures.

Based on Fig. 6, it can be seen that there were only minor changes in the breakout angular span throughout the process. This indicates that the breakout angular span may form quickly at an early stage of the breakout and does not widen significantly with time. The observation here agrees with earlier studies in which breakout angular span can be assumed constant and considered as a reliable parameter for horizontal stress estimation [2,18,22,26,27,62]. Followed by the approach proposed by Barton et al. [6], the breakout angular span has been widely used to constrain or compute the horizontal stress magnitudes provided that the downhole logging data is available [6,7,10–12,63–69].

Unlike the breakout angular span, the breakout depth tended to propagate along the σ_h direction and elongated at various stages of the simulation (see Fig. 6). The breakout tip gradually got narrower and finally formed a "V-shaped" or "dog-ear" shaped breakout. The progressive breakout development agrees with various researchers [2,6,20,24,41,49] and the similar phenomena were reported in both laboratory and field cases [27–29]. Breakout depth may not be an effective parameter for stress estimation based on a simple elastic solution e.g. Kirsch solution, as it is practically impossible to measure the breakout depth when it was just formed. Zoback et al. [2] and Barton et al. [6] have discussed this limitation in their studies as well. Hence, an unconventional methodology e.g. machine learning or neural network, may utilize the breakout depth data and solve this problem [70]. Lin et al. [71] have collected extensive laboratory and field data from literature and mine site for this purpose. Fig. 7 shows the angular span obtained from numerical simulation against the experimental data. As illustrated in Fig. 7, the numerical angular span follows a similar trend as the laboratory investigation, i.e. the higher stress ratio (the higher maximum horizontal stress) would result in a wider breakout angular span given the constant minimum horizontal and vertical stresses. Results again confirm that there is a definite relationship between the maximum horizontal stress and angular span.

It is noteworthy that the breakout angular spans produced with different borehole radius were different under the exact same stress conditions: the larger borehole radius yields a wider breakout. This is also in line with the experimental observation, which contradicts the Kirsch solution as the stress conditions at a given point along the borehole wall should be the same if the same boundary stresses are applied. As discussed earlier, the phenomenon is primarily due to the influence of the borehole size, in which the smaller borehole size requires higher stress concentration to nucleate breakout [24,48,49,72–74]. Therefore, the simulation results show that the PFC2D can effectively take account of the borehole size effect, as discussed in Section 4.2.

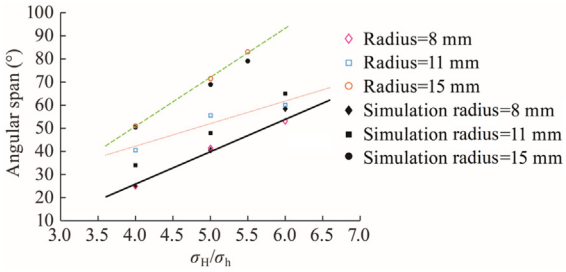

Fig. 7. Simulation results on breakout angular span vs. the experimental results.

4.2. Borehole size effect

Borehole size is an important parameter that should be considered in the laboratory study as it can significantly intensify the stress required for breakout initiation [73]. A series of studies have attempted to investigate this mechanism [14,75–78], popular explanations include the stress averaging concept [72,79–81], fracture mechanics [82] and conservation of energy [49]. As observed previously, the horizontal stress ratios used in the laboratory conditions were generally greater than that in the field conditions unless it is under high differential stress. For instance, Haimson & Herrick [13] applied a horizontal stress ratio over 10 in some of their experimental work. This is highly unlikely to be seen in the field.

4.2.1. Simulation procedures and breakout initiation stress

A numerical study on borehole size effect was also carried out in PFC2D in which the pre-drilled specimen was loaded under a hydrostatic compressive condition. In total, there were six different borehole radii investigated, ranging from 2 to 12 mm. As suggested by Lotidis et al. [83], the onset breakout initiation in PFC2D can be defined when there is a non-linear deflection in the stress-strain curve combined with a sudden increase in cumulative microcrack numbers. In laboratory conditions, this is generally defined by strain gauges and acoustic emission [48,72,84–87]. The same approach was also adopted in the numerical simulation via PFC2D by Duan & Kwok [24].

According to the Kirsch solution [88], the stress around a borehole can be expressed as follows.

$$\sigma_r = \left(1 - R^2/r^2\right)(\sigma_H + \sigma_h)/2 + \left(1 - 4R^2/r^2 + 3R^4/r^4\right)\cos 2\theta(\sigma_H - \sigma_h)/2 + \Delta P R^2/r^2 \quad (1)$$

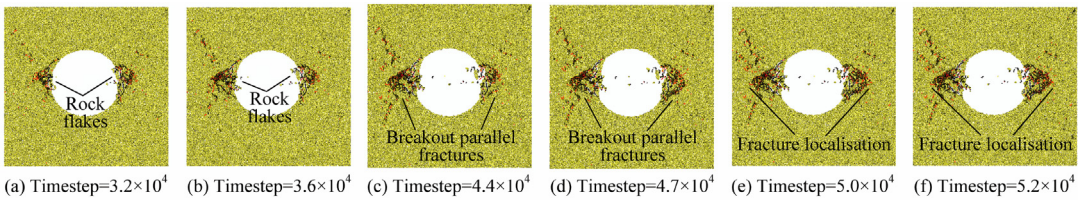

Fig. 6. Breakout development at various stages under σ_H = 50 MPa and σ_h = 10 MPa with 15 mm radius.

$$\sigma_\theta = \left(1 + R^2/r^2\right)(\sigma_H + \sigma_h)/2 - \left(1 + 3R^4/r^4\right)\cos 2\theta(\sigma_H - \sigma_h)/2 - \Delta P R^2/r^2 \quad (2)$$

where σ_θ is the tangential stress; σ_r the radial stress; R the borehole size; r the distance from the centre of the borehole to the point of interest; and ΔP the difference between mud pressure and pore pressure. A series of researchers have argued that the breakout would initiate at the maximum tangential stress concentration location [13,14,46,48], where the tangential stress can be estimated as

$$\sigma_\theta = 3\sigma_H - \sigma_h \quad (3)$$

Under hydrostatic conditions, the tangential stress around the borehole can be simplified as

$$\sigma_\theta = \left(1 + R^2/r^2\right)(\sigma_H + \sigma_h)/2 = \sigma_P \quad (4)$$

where σ_P is the hydrostatic pressure applied in the model. For an isotropic material, the breakout would initiate around the borehole at the same time. Fig. 8a illustrates the simulation of 6 mm borehole radius and the breakout initiation stress (the red circled point is the breakout initiation stress with the value of 58.7 MPa) is labelled. A non-linear deflection can be observed at the stress, indicating the onset breakout initiation [24,83–85]. At the same time, crack numbers around borehole increased substantially, as seen in Fig. 8b. This is in good agreement with the simulation from Duan & Kwok [24]. Fig. 8c and d show the model states prior and after the breakout initiation, respectively. It can be found that extensive cracks generated after the initiation stress, which was dominated by tensile cracks. This was in good agreement with Fig. 8a and b, confirming that the stress-strain curve deflection can be used as the breakout initiation indication. It is worth noting that the cracks are not uniformly distributed around the borehole; this is mainly due to the heterogeneity of the DEM model.

Although Duan & Kwok [24] also conducted borehole size effect investigation using PFC, the maximum borehole diameter used was 16 mm, which was almost 1/3 of their specimen length (50 mm). Boundary effect can have significant effect under this ratio and influence the breakout initiation stress considerably. Therefore, the conclusions from Duan & Kwok [24] might be tentative, especially for boreholes that had diameters over 10 mm. This might be the reason why the lower breakout initiation stresses were observed by Duan & Kwok [24] comparing with experimental studies. On the other hand, the numerical simulation on borehole size effect in this study covered a wider range of borehole diameters up to 24 mm while keeping the ratio between borehole diameter and specimen length under 1/5. In this case, the boundary effect on simulation results can be eliminated.

4.2.2. Implications on stress averaging model

As proposed by Lajtai [79] and Carter [48], the intensification of breakout initiation stress is due to the stress averaging concept, which the stress under the high gradient is redistributed towards the lower area over a distance. This critical distance (d) is considered as a material constant and is determined based on the curve fitting data. As suggested by Carter et al. [89], the critical distance varies between 2 and 3.5 mm from ductile to brittle material. Although the stress averaging phenomenon can be identified through strain distributions obtained from strain gauges along surface of the borehole [48], it does not explicitly show the stress transfer along the distance. The measurement circle function embedded in PFC measures the stress change within the predefined circle during the simulation process. Hence, six 1 mm diameter measurement circles were assigned parallel and perpendicular to the minimum horizontal principal stress direction to cover the possible averaging distance and monitor the stress averaging phenomenon numerically, as illustrated in Fig. 9. Fig. 10a shows the tangential stress in measurement circles 1–3. It can be seen from Fig. 10a that the tangential stress in circle 1 was approximately 2 times of the applied hydrostatic stress (σ_P) prior to point A, which agrees with Eq. (4). Clear stress re-distribution between circles can be observed after this point and eventually led to substantial stress reduction in circle 1 at point B; this point also happens to be the breakout initiation stress point in Fig. 8a, which further confirms this methodology of analyzing borehole size effect through PFC. On the other hand, stress averaging seems taking place between the two points as the tangential stress within circles tend to approach similar values. It is also worth noting that the deflections in stress-strain curves are corresponding to the formation of micro-cracks since the deflection points in Fig. 10a well matched with increasing crack numbers in Fig. 8b, such that the measurement circle might be also used as a complementary indication tool for breakout initiation detection in PFC. The implication here is that the stress averaging is perhaps due to the energy release through micro-cracking, which was also discussed by some studies [90,91].

Fig. 10b illustrates the radial stress in measurement circles 1–3. The magnitude of radial stress in circle 1 was relatively small comparing with other stresses, which is in line with Eq. (1). Some degree of stress transfer between circles can also be found after the same point A in Fig. 10a, although the radial stress magnitude in circle 3 was marginally greater than that of circles 1 and 2. Based on the results in Fig. 10a and b, it implies that the stress averaging distance of the material might be within the distance of 2–3 mm, which is in good agreement with the experimental observations from Carter et al. [89]. Similar to the tangential stress, there is also a significant drop in radial stress at the point B, which again indicates the on-set breakout initiation. The magnitude of radial stress can be as high as 10 to 20 MPa prior to the on-set breakout initiation, as shown in Fig. 10b. Hence, it is be important to consider the influence of radial stress during the estimation of breakout initiation stress from stress averaging concept. In addition, the numerical model may be further improved to simulate the phenomenon in more detail since it only considers the failure of bonding material instead of particle breakage. A grain-based model incorporating

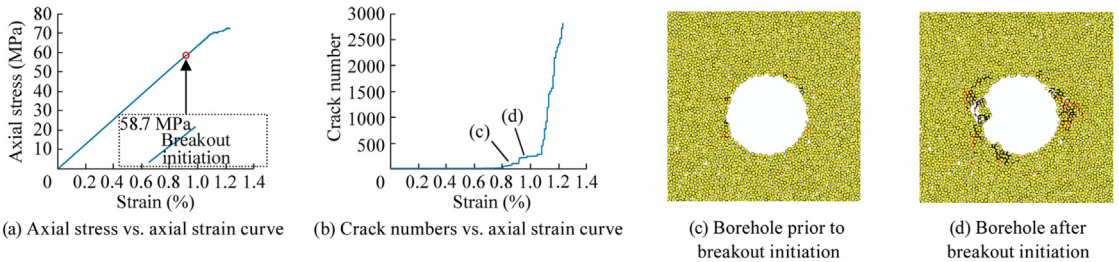

(a) Axial stress vs. axial strain curve (b) Crack numbers vs. axial strain curve (c) Borehole prior to breakout initiation (d) Borehole after breakout initiation

Fig. 8. Borehole size test at 6 mm borehole radius.

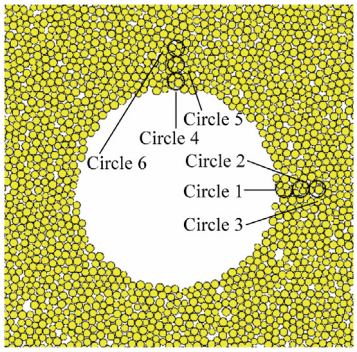

Fig. 9. Stress measurement circle positions around 6 mm radius borehole.

both intra- and extra-granular failure should be implemented in the future studies to take account of the micro-crack within the grain.

Fig. 10c and d show the tangential and radial stress in measurement circles 4–6, respectively. An overall agreement can be observed between stresses in circles 1–3 and circles 4–6, in which stress re-distribution started at about point A with lower change in magnitudes. It was found that there was not significant stress reduction at point B and breakout initiation occurred at the left and right sides of the borehole first (see Fig. 8d). This is because the DEM model is heterogeneous and stress is not evenly distributed around the borehole.

4.2.3. Implications on pressure-dependent linear elastic model

Santarelli et al. suggested that Young's modulus of rock is not constant but rather depends on the confinement [92]. In this case, the Young's modulus is higher into the rock due to higher radial stress. This leads to relocation of the maximum tangential stress from the borehole wall to the rock, namely, pressure-dependent linear elastic model. Hence, Santarelli & Brown suggested that breakout initiation should occur at some distance from the borehole wall instead of the surface of borehole [93].

In Fig. 10a, it can be seen that the tangential stress in circle 2 surpassed that in circle 1 during the loading stage prior to any cracking and the substantial stress reduction happened in both circles 1 and 2 at the same time. This might indicate the maximum tangential stress relocation around borehole and breakout initiation at some distance from the borehole. However, this was not observed in measurement circles 4–6. Thereby, it is noticed that majority of micro-cracking started around the borehole at the borehole wall rather than some distance into the rock (see Fig. 8c and d). This is not in line with the proposed breakout initiation location from pressure-dependent linear elastic model.

Although there might be the tangential stress relocation due to change in Young's modulus, it is practically difficult to have fracture initiation into the rock due to the stress state. As presented by Santarelli et al. [92], for 100 MPa hydrostatic pressure, the maximum tangential stress would be approximately 125 MPa at the distance that is 1.5 times of radius away from the center of the borehole based on the model; whereas the tangential stress at the borehole wall is 100 MPa. However, the radial stresses at the two locations are considerably different under 100 MPa pressure. At the borehole wall, the radial stress can be neglected, whereas at the maximum tangential stress location, the magnitude of radial stress can be over 50 MPa based on the Kirsch solution. This means the breakout initiation would occur at the borehole wall due to its low confinement even considering the pressure-dependent linear elastic model. On the other hand, the breakout initiation might happen at the location into the rock if the distance is very small from the borehole wall, so that the magnitude of radial stress is minimal and can be neglected. This distance is rather difficult to be determined and requires further investigation.

4.2.4. Comparison with experimental results

Fig. 11 displays the simulation results against the previous experimental studies from normal compression and hollow cylinder tests, where the critical tangential stresses were estimated from Eqs. (3) and (4). According to Fig. 11, it can be seen that the simulation results are well aligned with literature data, which shows a decreasing trend with larger borehole radius. The decreasing trend tends to be steadier once the borehole radius is greater than 6 mm, whereas sharper drop can be seen at smaller radii. As observed in the trend, it might be possible to derive an empirical relationship to estimate the breakout initiation stress based on two sets of data (normal compression and hollow cylinder tests).

In addition, it seems that the ratios that obtained from normal compression tests are slightly lower than that of the hollow cylinder tests given the same borehole radius. It is suspected that this is perhaps due to the size of the rock sample. In hollow cylinder tests, the specimen size is usually fixed with various borehole sizes. On the other hand, different specimen sizes were used in the normal compression tests, i.e. the larger the borehole radius, the larger the sample size. As discussed in many studies, different sample sizes already include the rock strength reduction due to the scale effect, in which smaller samples have higher strength than larger samples [94–96]. Correspondingly, this may influence the borehole size effect investigation and increase the critical breakout initiation stress for smaller specimens. To verify the influence of the sample size and isolate the borehole size parameter, a systematic laboratory study is proposed for future studies.

4.3. Thermal effects on borehole size and borehole breakout

As exploitation activities including mining and geothermal wells are inevitably going deeper, the surrounding rock temperature also increases accordingly [34,35]. As discussed by a series of researchers [97–100], the temperature has impact on the rock mechanical behavior. It is suspected that the borehole breakout initiation stress and breakout angular span may also be affected

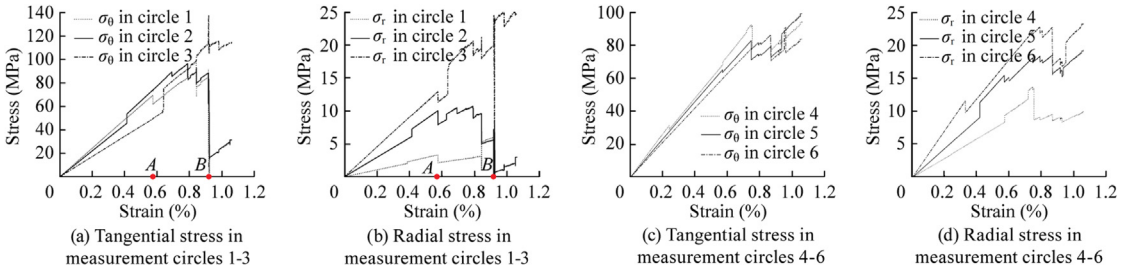

Fig. 10. Tangential and radial stresses within the measurement circles.

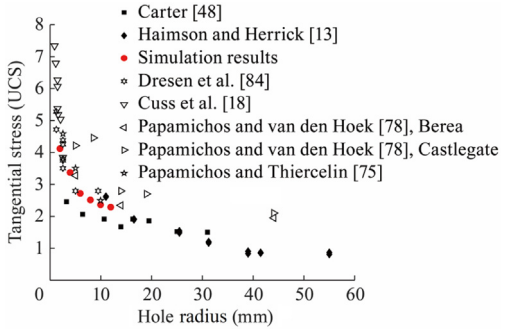

Fig. 11. The ratio between critical tangential stress at breakout initiation vs. UCS from both literature and numerical simulation, where the black filled data are normal compression test data.

by high temperature and interrupt the horizontal stress estimation. However, it is difficult to perform triaxial tests under the high temperature in a laboratory environment. Formerly, the thermal related studies on rock specimens have been carried out via PFC2D. Therefore, it was also utilized to investigate the breakout angular span under various temperatures.

4.3.1. Thermal contact model

In PFC2D, the thermal analysis does not require any calibration of micro-parameters and these parameters can be directly assigned to the synthetic specimen. The thermal material consists of a network of "heat reservoirs (particles)" that are connected by "thermal pipes (contacts)". The thermal pipes enable the heat transfer between reservoirs through heat conduction and are governed by the thermal pipe contact model. In the model, each pipe can be represented by a one-dimensional entity with associated power (Q) to reflect the heat flux [37,50]. Q can be calculated and updated by

$$Q = \Delta T/\eta L \tag{5}$$

where ΔT is the temperature difference between the two reservoirs connected by a pipe; L the length of the pipe; η the thermal resistance per unit length, which is used to describe the macro-isotropic thermal conductivity (k) of a material. The relationship between the two parameters can be expressed as

$$\eta = \sum_{N_p} l_p\left((1-n)/\sum\nolimits_{N_b} V_b\right)/2k \tag{6}$$

where n is the porosity in the volume of interest; N_b the number of particles within the region; N_p the number of thermal pipes within the region; V_b the volume of a particle; and l_p the length of a thermal pipe. The heat-conduction equation for each reservoir is defined as

$$-\sum_{p=1}^{N} Q_p + Q_v = mC_v\partial T/\partial t \tag{7}$$

where Q_v is the heat-source power; Q_p the power of each thermal pipe that is flowing out of the reservoir; m the thermal mass; and C_v the specific heat. In PFC2D, the thermally induced change of particle size and bonding forces are considered to represent the thermal strain. The temperature variation results in the particle radius expansion, which can be calculated by

$$\Delta R = \alpha R \Delta T \tag{8}$$

where ΔR is the change in particle radius due to temperature change; and α the thermal expansion coefficient of particles. The thermal expansion of the bonding material can be denoted as the change in the normal force ($\Delta\bar{F}_n$) of the bond.

$$\Delta\bar{F}_n = -k_n A\left(\bar{\alpha}\,\bar{L}\,\Delta T\right) \tag{9}$$

where k_n is the normal stiffness of the bond; A the cross-section area of the bond; $\bar{\alpha}$ the average thermal expansion coefficients of the two particles on each end of the bond; and $\bar{L}$ the bond length.

4.3.2. Simulation procedures

To accurately simulate the breakout generated under the thermal effect, the appropriate thermal properties of Gosford sandstone were selected. The specific heat was assigned to be 790 J/kg °C and the thermal expansion coefficient was 1.3×10^{-5} K^{-1} [101]. According to Abdulagatova et al., the thermal conductivity of the specimen was chosen as 3.75 $Wm^{-1}K^{-1}$ [102]. Once the rock was created, it was gradually heated inwards to reach the pre-set temperature (see Fig. 12). By then, the standard procedures discussed in Sections 3.3 and 4.2 were followed to apply horizontal stresses to the sample. This aims to keep consistency between simulations to allow direct comparisons between the results produced with and without the thermal effect. To investigate the corresponding thermal effect that could possibly be encountered at deep locations, four scenarios were considered with temperatures ranging from 100 to 400 °C.

4.3.3. Thermal influence on borehole size effect

A total number of 20 simulations were conducted from 4 to 12 mm borehole sizes to investigate the influence of temperature on breakout initiation stress. Fig. 13 displays the results obtained from the numerical simulation. Overall, a decreasing trend of breakout initiation stresses with increasing temperatures can be observed. The rates of deduction are higher for 4 and 6 mm borehole sizes comparing with the larger borehole sizes, suggesting the temperature has some degree of influence on breakout initiation stress, especially for smaller borehole sizes. On the other hand, the change in the stress in larger borehole sizes (8–12 mm) are minimal and may be neglected since the reduction can be as small as 5%. It is noticed that the axial stress required for 8 mm was higher than 6 mm under 300 and 400 °C. As discussed earlier, the synthetic rock generated in DEM model is not isotropic. Due to the randomness of particle size distribution, there are locations around the borehole that contained larger particles, such that micro-cracking will occur in these locations first, as shown in Fig. 8c and d. Under the temperature effect, particles expanded and created additional contact force to bonds. This can induce stress localisation at places where particles are larger, so that the breakout initiation can occur at lower stress for 6 mm borehole radius under higher temperature.

Fig. 14a–e display the proportion of tensile to shear cracks under different temperatures. A general decreasing trend of the ratio can be seen from Fig. 14, implying that as temperature increases, the micro-cracking mode gradually transfers from ten-

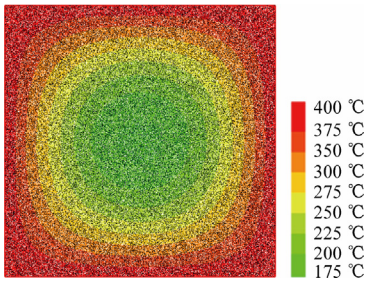

Fig. 12. Sample heating under 400 °C temperature.

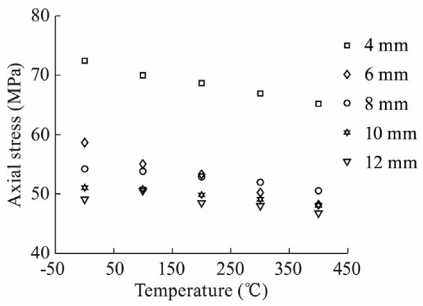

Fig. 13. Axial stresses for on-set breakout initiation under various temperatures.

sile cracking to shear cracking, except under 10 mm borehole size, where the ratio fluctuated with temperature. Similar to the breakout initiation stress, the decrease in ratio is more significant under 4 and 6 mm borehole sizes than that of the larger borehole sizes. The implication here is there might be a correlation with the two parameters, although further investigation is required. Fig. 14f shows the crack ratio with different borehole size neglecting the influence of temperature. It is noted that the crack ratio under 4 mm borehole size is substantially lower than the others, whereas the ratio under other borehole sizes are quite consistent with minor difference. This is also true for the ratios under other temperatures, as depicted in Fig. 14a–e. It is suspected that this low crack ratio might contribute to the breakout initiation stress since the stress required to initiate breakout with 4 mm borehole size is marginally higher than that of others, as displayed in Fig. 13. However, further study is also required to confirm this hypothesis. Overall, it can be seen that the temperature has influence on the micro-cracking mode, which may subsequently affect the breakout initiation stress.

4.3.4. Thermal influence on borehole breakout

The above section analysed the initiation stress, whereas this section will focus on the influence on breakout angular span as it is the most critical parameter for horizontal stress constraint and estimation. Numerical simulations were conducted under different temperatures and results can be seen in Fig. 15. Under lower σ_H (40 MPa), the breakout angular span remains relatively constant regardless of the temperature change, whereas the breakout angular span increased considerably at 300 and 400 °C for higher σ_H (50 MPa). It is also noticed that the change between 300 and 400 °C is minimal. This implies that the thermal effect may have influence on the breakout angular span under a higher horizontal stress condition when the temperature is over 300 °C.

Fig. 16 shows the simulation results with 11 mm borehole size under 50 MPa of σ_H, where the base case (no temperature) is displayed in Fig. 6. The breakout orientations under 100 and 200 °C are consistent with the simulation without the temperature (see Fig. 16a and b). However, the breakout orientation changed under the higher temperature (see Fig. 16c and d). A similar orientation change was also observed with 8 mm borehole size under 50 MPa of σ_H. This is perhaps due to the thermal related micro-cracks generated during the breakout formation, as particles expand during the heating process which may lead to increased contacting force in local areas. For instance, micro-cracks started to appear and become dense around the top right side of the borehole as temperature increases, which was not observed under 0 and 100 °C. Hence, the local micro-cracking due to temperature effect subsequently altered the breakout orientations as well as angular span under higher temperature. The implication here is that the temperature might be considered for the determination of horizontal stress orientation and magnitudes for borehole breakout collected from geothermal wells.

The simulation shows that there might be some degree of influence on breakout angular span and orientation under the high temperature (300 °C) and high horizontal stress condition (50 MPa). Although this requires further investigation and consideration, especially for deep geothermal wells where the temperature can be as high as 500 °C [103]. On the other hand, the underground temperatures in coal mining areas are relatively low. For instance, He reported that the average temperature in 33 coal mines with depth of cover over 1000 m is between 30 to 40 °C [104], whereas Yang et al. summarized the information in numerous studies in China, as shown in Table 3 [105]. Therefore, thermal effect on breakout angular span may not need to be considered under these scenarios.

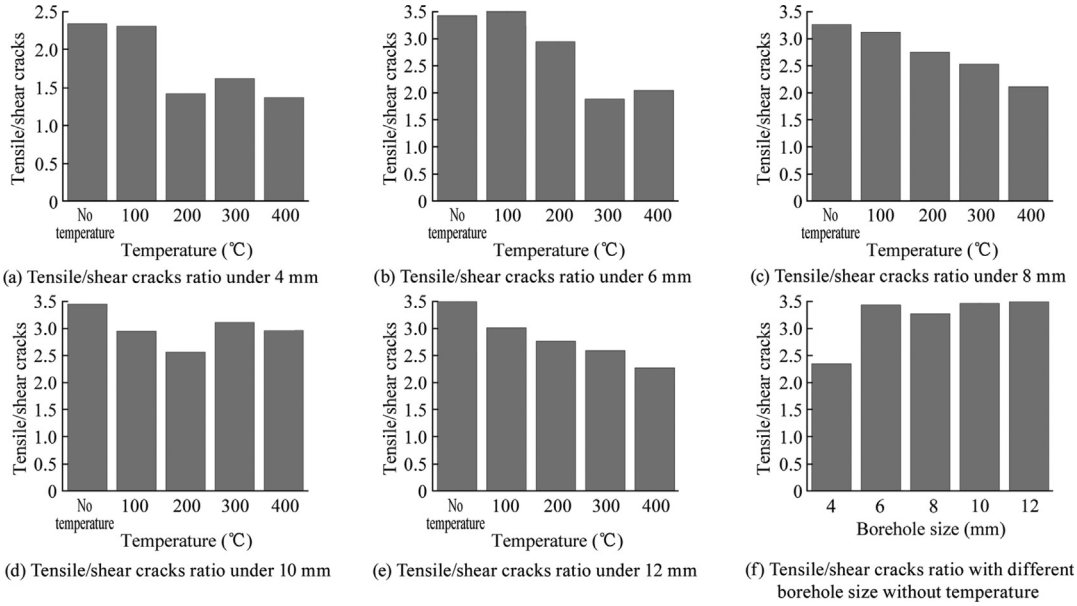

(a) Tensile/shear cracks ratio under 4 mm
(b) Tensile/shear cracks ratio under 6 mm
(c) Tensile/shear cracks ratio under 8 mm
(d) Tensile/shear cracks ratio under 10 mm
(e) Tensile/shear cracks ratio under 12 mm
(f) Tensile/shear cracks ratio with different borehole size without temperature

Fig. 14. Tensile/shear cracks ratios under different borehole sizes and different temperatures.

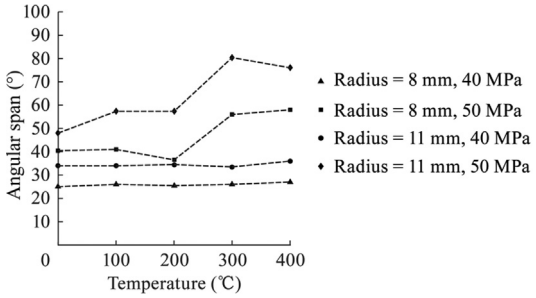

Fig. 15. Simulation results under various conditions.

Table 3
Mine site temperature collected from literature [105].

Mine site name	Depth of cover (m)	Underground temperature (°C)
Sanhejian	1300	56
Jiahe	800	32–34
Zhangshuanglou	1000	34–36
Zhangxiaolou	1125	30
Jisan	785	31–51
Wobei	640	35–37
Yongchuan	800	29.3–31.5

5. Conclusions

The breakout geometrical variation under different stress conditions was studied numerically. Laboratory results revealed that breakout geometries are closely related to horizontal stress magnitudes as well as the borehole size. Both higher maximum horizontal stress and larger borehole radius can result in deeper and wider breakout given the same other parameters. The implication is that there is a relationship between breakout geometries and horizontal stress magnitudes.

The DEM model result shows similar breakout behavior as discussed above. Based on the numerical simulations, it is clear that the breakout angular span forms at a very early stage of the breakout and does not widen significantly, which is then followed by subsequent fracture propagation along the minimum horizontal stress direction. The results agree with the argument mentioned in various studies and indicated that breakout angular span can be used as a reliable indicator of horizontal stress estimation. Due to the complexity of breakout depth development and its relationship with horizontal stress magnitudes, it is difficult to derive a simple analytical method for stress estimation. Therefore, it may be useful to consider an unconventional approach either through time-dependent numerical simulations or advanced computer techniques, including machine learning or neural networks. For instance, a massive database may be used to train the machine to correlate between breakout depth and horizontal stress magnitudes given the vast breakout data available in place.

In addition, the relationship between the breakout initiation stress and borehole size was also investigated in this study. Simulation results are well in line with the previous experimental observations in which the smaller borehole size can amplify the breakout initiation stress considerably. The stress analysis around the borehole also shows some degree of stress averaging from micro-cracking and the importance of radial stress. Therefore, borehole size is a critical parameter in laboratory borehole breakout study and the stress averaging approach should not ignore the influence of radial stress.

It is worth noting that micro-cracking occurred at the borehole wall rather than some distance into the rock and the borehole breakout initiation is likely to occur at borehole wall even considering the pressure-dependent linear elastic model. However, further investigation is required to confirm this observation.

Based on the analysis of previous data, it was found that the ratios of breakout initiation and UCS in normal compression test were slightly lower than that of the hollow cylinder tests. It might be resulted from the rock strength variation due to scale effect as the normal compression tests used various specimen sizes. However, due to the limited data numbers, this conclusion is rather tentative. Hence, a systematic laboratory approach is currently undertaken to study the influence of specimen size on the breakout initiation stress.

In this study, the thermal effect on borehole size and borehole breakout was investigated. Results showed that the breakout initiation stress reduces with increasing temperature, although it may be neglected for borehole size over 6 mm. The more proportion of shear cracks was induced as temperature increases, which may also contribute to the decrease in breakout initiation stress. For thermal effect on borehole breakout, it can be seen that under the lower maximum horizontal stress, the temperature only has a minor influence on breakout. Conversely, the higher horizontal stress resulted in a significantly wider breakout angular span when the temperature is over 300 °C. The corresponding breakout orientation also varies under these scenarios. This implies that the thermal effect may need to be taken into account under high temperature and high horizontal stress conditions when using breakout angular span for horizontal stress constraint or estimation, especially in geothermal wells. However, the temperature in most underground coal mines is relatively low, suggesting the thermal effect may be neglected in this case.

Acknowledgement

The work reported here is funded by Australian Coal Industry's Research Program (ACARP) grant no. C26063.

References

[1] Martin CD. Seventeenth Canadian geotechnical colloquium: The effect of cohesion loss and stress path on brittle rock strength. Can Geotech J 1997;34(5):698–725.
[2] Zoback MD, Moos D, Mastin L, Anderson RN. Well bore breakouts and in situ stress. J Geophys Res 1985;90(B7):5523–30.

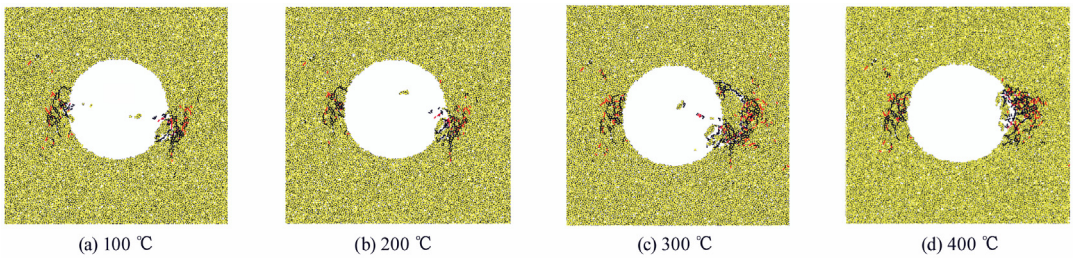

Fig. 16. Breakout generated under different temperatures at 11 mm borehole radius.

[3] Jarosiński M. Ongoing tectonic reactivation of the Outer Carpathians and its impact on the foreland: Results of borehole breakout measurements in Poland. Tectonophysics 2005;410(1–4):189–216.
[4] Fowler MJ, Weir FM. The use of borehole breakouts for geotechnical investigation of an open pit mine. In: Proceedings of the 1st Southern hemisphere international rock mechanics symposium. Perth; 2008.
[5] Ask MVS, Ask D, Elvebakk H, Olesen O. Stress Analysis in Boreholes Drag Bh and Leknes Bh, Nordland, North Norway. Rock Mech Rock Eng 2015;48(4):1475–84.
[6] Barton CA, Zoback MD, Burns KL. In-situ stress orientation and magnitude at the Fenton Geothermal Site, New Mexico, determined from wellbore breakouts. Geophys Res Lett 1988;15(5):467–70.
[7] Chang C, McNeill LC, Moore JC, Lin W, Conin M, Yamada Y. In situ stress state in the Nankai accretionary wedge estimated from borehole wall failures. Geochem Geophys Geosyst 2010;11(12)::Q0AD04.
[8] Tingay MRP, Hillis RR, Morley CK, King RC, Swarbrick RE, Damit AR. Present-day stress and neotectonics of Brunei: Implications for petroleum exploration and production. Am Assoc Pet Geol Bull 2009;93(1):75–100.
[9] Haimson B. Micromechanisms of borehole instability leading to breakouts in rocks. Int J Rock Mech Min Sci 2007;44(2):157–73.
[10] Zoback MD, Barton CA, Brudy M, Castillo DA, Finkbeiner T, Grollimund BR, et al. Determination of stress orientation and magnitude in deep wells. Int J Rock Mech Min Sci 2003;40(7–8):1049–76.
[11] Vernik L, Zoback MD. Estimation of maximum horizontal principal stress magnitude from stress-induced well bore breakouts in the Cajon Pass scientific research borehole. J Geophys Res 1992;97(B4):5109–19.
[12] Song I, Chang C. Stochastic Optimization of In Situ Horizontal Stress Magnitudes Using Probabilistic Model of Rock Failure at Wellbore Breakout Margin. Rock Mech Rock Eng 2018;51(9):2761–76.
[13] Haimson HC, Herrick CG. Borehole breakouts - a new tool for estimating in situ stress? In: Proceedings of the International Society for Rock Mechanics and Rock Engineering ISRM International Symposium. Stockholm; 1986.
[14] Haimson BC, Herrick CG. Borehole breakouts and in situ stress. In: Proceedings of the 12th annual energy-sources technology conference and exhibition. Houston, New York: American Society of Mechanical Engineers; 1989.p.17-22.
[15] Haimson BC, Song I. Laboratory study of borehole breakouts in Cordova Cream: a case of shear failure mechanism. Int J Rock Mech Min Sci 1993;30(7):1047–56.
[16] Lee H, Haimson BC. Borehole breakouts and in-situ stress in sandstones. In: Proceedings of the International Symposium on In-Situ Rock Stress. Trondheim: CRC Press; 2006.p.201.
[17] Haimson B, Kovacich J. Borehole instability in high-porosity Berea sandstone and factors affecting dimensions and shape of fracture-like breakouts. Eng Geol 2003;69(3–4):219–31.
[18] Cuss RJ, Rutter EH, Holloway RF. Experimental observations of the mechanics of borehole failure in porous sandstone. Int J Rock Mech Min Sci 2003;40(5):747–61.
[19] Haimson B, Lee H. Borehole breakouts and compaction bands in two high-porosity sandstones. Int J Rock Mech Min Sci 2004;41(2):287–301.
[20] Lee H, Moon T, Haimson BC. Borehole breakouts induced in arkosic sandstones and a discrete element analysis. Rock Mech Rock Eng 2016;49(4):1369–88.
[21] Haimson BC, Lee M, Herrick C. Recent advances in in-situ stress measurements by hydraulic fracturing and borehole breakouts. In: Proceedings of the 7th ISRM Congress. Aachen: International Society for Rock Mechanics and Rock Engineering; 1991.p.1737-42.
[22] Herrick CG, Haimson BC. Modeling of episodic failure leading to borehole breakouts in Alabama limestone. In: Proceedings of the 1st North American Rock Mechanics Symposium, NARMS 1994. Austin: American Rock Mechanics Association; 1994.p.217-24.
[23] Sahara DP, Schoenball M, Gerolymatou E, Kohl T. Analysis of borehole breakout development using continuum damage mechanics. Int J Rock Mech Min Sci 2017;97:134–43.
[24] Duan K, Kwok CY. Evolution of stress-induced borehole breakout in inherently anisotropic rock: Insights from discrete element modeling. J Geophys Res Solid Earth 2016;121(4):2361–81.
[25] Stock JM, Healy JH, Hickman SH, Zoback MD. Hydraulic fracturing stress measurements at Yucca Mountain, Nevada, and relationship to the regional stress field (USA). J Geophys Res Solid Earth 1985;90(B10):8691–706.
[26] Schoenball M, Sahara DP, Kohl T. Time-dependent brittle creep as a mechanism for time-delayed wellbore failure. Int J Rock Mech Min Sci 2014;70:400–6.
[27] Mastin LG. An analysis of stress-induced elongation of boreholes at depth. Master's dissertation. Stanford University; 1984.
[28] Plumb RA, Hickman SH. Stress-induced borehole elongation: A comparison between the four-arm dipmeter and the borehole televiewer in the Auburn geothermal well. J Geophys Res Solid Earth 1985;90(B7):5513–21.
[29] Kessels W. Observation and interpretation of time-dependent behaviour of boreholes stability in the continental deep drilling pilot borehole. In: Proceedings of the ISRM International Symposium. Pau: International Society for Rock Mechanics and Rock Engineering; 1989.p.1479-86.
[30] Ranjith PG, Zhao J, Ju M, De Silva RV, Rathnaweera TD, Bandara AKMS. Opportunities and challenges in deep mining: a brief review. Engineering 2017;3(4):546–51.
[31] Xie HP, Gao F, Ju Y, Gao MZ, Zhang R, Gao YN, et al. Quantitative definition and investigation of deep mining. J China Coal Soc 2015;40(1):1–10.
[32] Xie H. Research framework and anticipated results of deep rock mechanics and mining theory. Adv Eng Sci 2017;49(2):1–16.
[33] Hu S, Peng J, Huang C, Chen P, Li M. An overview of current status and progress in coal mining of the deep over a kilometer. China Mining Mag 2011;20(7):105–10.
[34] Gürtunca RG. Mining below 3000m and challenges for the South African gold mining industry. Mechanics of Jointed and Faulted Rock. Rotterdam:A.A. Balkema; 2018.p.3-10.
[35] Al Sayed C, Vinches L, Hallé S. Towards optimizing a personal cooling garment for hot and humid deep mining conditions. Open J Optim 2016;5(1):35–43.
[36] Yang L, Marshall AM, Wanatowski D, Stace R, Ekneligoda TC. Effect of high temperatures on sandstone - a computed tomography scan study. Int J Phys Modell Geotech 2017;17(2):75–90.
[37] Wanne TS, Young RP. Bonded-particle modeling of thermally fractured granite. Int J Rock Mech Min Sci 2008;45(5):789–99.
[38] Zhao XG, Xu HR, Zhao Z, Guo Z, Cai M, Wang J. Thermal conductivity of thermally damaged Beishan granite under uniaxial compression. Int J Rock Mech Min Sci 2019;115:121–36.
[39] Gomar M, Goodarznia I, Shadizadeh SR. Transient thermo-poroelastic finite element analysis of borehole breakouts. Int J Rock Mech Min Sci 2014;71:418–28.
[40] Cui Y, Nouri A, Chan D, Rahmati E. A new approach to DEM simulation of sand production. J Petrol Sci Eng 2016;147:56–67.
[41] Shen B, Stephansson O, Rinne M. Simulation of borehole breakouts using FRACOD^{2D}. Oil Gas Sci Technol 2002;57(5):579–90.
[42] Crook T, Willson S, Yu JG, Owen R. Computational modelling of the localized deformation associated with borehole breakout in quasi-brittle materials. J Petrol Sci Eng 2003;38(3–4):177–86.
[43] Cook B, Lee M, DiGiovanni A, Bronowski D, Perkins E, Williams J. Discrete element modeling applied to laboratory simulation of near-wellbore mechanics. Int J Geomech 2004;4(1):19–27.
[44] Zhang H, Yin S, Aadnoy BS. Poroelastic modeling of borehole breakouts for in-situ stress determination by finite element method. J Petrol Sci Eng 2018;162:674–84.
[45] Cheng W, Jiang G, Zhou Z, Wei Z, Li X. Numerical simulation for the dynamic breakout of a borehole using boundary element method. Geotech Geol Eng 2019;37(4):2873–81.
[46] Lin H, Oh J, Canbulat I, Stacey TR. Experimental and analytical investigations of the effect of hole size on borehole breakout geometries for estimation of in situ stresses. Rock Mech Rock Eng 2020;53(2):781–98.
[47] Haimson BC, Song I. Borehole breakouts in Berea sandstone: two porosity-dependent distinct shapes and mechanisms of formation. In: Proceedings of the SPE/ISRM Rock Mechanics in Petroleum Engineering Conference. Trondheim; 1998.p.229-38.
[48] Carter B. Size and stress gradient effects on fracture around cavities. Rock Mech Rock Eng 1992;25(3):167–86.
[49] Bažant ZP, Lin FB, Lippmann H. Fracture energy release and size effect in borehole breakout. Int J Numer Anal Meth Geomech 1993;17(1):1–14.
[50] Itasca. PFC 5.0 Documentation. Minneapolis Minnesota: Itasca Consulting Group Inc.; 2018.
[51] Vallejos JA, Salinas JM, Delonca A, Ivars DM. Calibration and verification of two bonded-particle models for simulation of intact rock behavior. Int J Geomech 2017;17(4):06016030.
[52] Bahaaddini M, Sheikhpourkhani AM, Mansouri H. Flat-joint model to reproduce the mechanical behaviour of intact rocks. Europ J Environ Civ Eng 2019:1–22.
[53] Zhao Z. Thermal influence on mechanical properties of granite:a microcracking perspective. Rock Mech Rock Eng 2016;49(3):747–62.
[54] Zhou J, Zhang L, Pan Z, Han Z. Numerical investigation of fluid-driven near-borehole fracture propagation in laminated reservoir rock using PFC2D. J Nat Gas Sci Eng 2016;36:719–33.
[55] Peter-Borie M, Blaisonneau A, Gentier S, Guillon T, Rachez X. Study of Thermo-Mechanical Damage around Deep Geothermal Wells: from the Micro-Processes to Macroscopic Effects in the Near Well. In: Proceedings of the World Geothermal Congress 2015. Melbourne; 2015.p.1-10.
[56] Fan X, Li K, Lai H, Xie Y, Cao R, Zheng J. Internal stress distribution and cracking around flaws and openings of rock block under uniaxial compression: A particle mechanics approach. Comput Geotech 2018;102:28–38.
[57] Potyondy DO, Cundall PA. A bonded-particle model for rock. Int J Rock Mech Min Sci 2004;41(S8):1329–64.
[58] Bahaaddini M, Sharrock G, Hebblewhite B. Numerical direct shear tests to model the shear behaviour of rock joints. Comput Geotech 2013;51:101–15.
[59] Yoon J. Application of experimental design and optimization to PFC model calibration in uniaxial compression simulation. Int J Rock Mech Min Sci 2007;44(6):871–89.
[60] Malinverno A, Saito S, Vannucchi P. Horizontal principal stress orientation in the Costa Rica Seismogenesis Project (CRISP) transect from borehole breakouts. Geochem Geophys Geosyst 2016;17(1):65–77.
[61] Lin W, Doan ML, Moore JC, McNeill L, Byrne TB, Ito T, et al. Present-day principal horizontal stress orientations in the Kumano forearc basin of the southwest Japan subduction zone determined from IODP NanTroSEIZE drilling Site C0009. Geophys Res Lett 2010;37(13):L13303.

[62] Zheng Z, Kemeny J, Cook NG. Analysis of borehole breakouts. J Geophys Res Solid Earth 1989;94(B6):7171–82.
[63] Brudy M, Zoback MD, Fuchs K, Rummel F, Baumgärtner J. Estimation of the complete stress tensor to 8 km depth in the KTB scientific drill holes: Implications for crustal strength. J Geophys Res Solid Earth 1997;102 (B8):18453–75.
[64] Huffman K, Saffer D. In situ stress magnitudes at the toe of the Nankai Trough Accretionary Prism, offshore Shikoku Island, Japan. J Geophys Res Solid Earth 2016;121(2):1202–17.
[65] Kim H, Xie L, Min KB, Bae S, Stephansson O. Integrated in situ stress estimation by hydraulic fracturing, borehole observations and numerical analysis at the EXP-1 Borehole in Pohang, Korea. Rock Mech Rock Eng 2017;50(12):3141–55.
[66] Zoback MD, Healy JH. In situ stress measurements to 3.5 km depth in the Cajon Pass scientific research borehole: Implications for the mechanics of crustal faulting. J Geophys Res: Solid Earth 1992;97(B4):5039–57.
[67] Yaghoubi AA, Zeinali M. Determination of magnitude and orientation of the in-situ stress from borehole breakout and effect of pore pressure on borehole stability - Case study in Cheshmeh Khush oil field of Iran. J Petrol Sci Eng 2009;67(3–4):116–26.
[68] Nian T, Wang G, Xiao C, Zhou L, Deng L, Li R. The in situ stress determination from borehole image logs in the Kuqa Depression. J Nat Gas Sci Eng 2016;34:1077–84.
[69] Molaghab A, Taherynia MH, Fatemi-Aghda SM, Fahimifar A. Determination of minimum and maximum stress profiles using wellbore failure evidences: a case study—a deep oil well in the southwest of Iran. J Pet Explor Prod Technol 2017;7(3):707–15.
[70] Zhang H, Yin S. Inference of in situ stress from thermoporoelastic borehole breakouts based on artificial neural network. Int J Numer Anal Meth Geomech 2019;43(16):2493–511.
[71] Lin H, Kang WH, Oh J, Canbulat I. Estimation of in-situ maximum horizontal principal stress magnitudes from borehole breakout data using machine learning. Int J Rock Mech Min Sci 2020;126:104199.
[72] Carter BJ, Lajtai EZ, Petukhov A. Primary and remote fracture around underground cavities. Int J Numer Anal Meth Geomech 1991;15(1):21–40.
[73] LeRiche AC. Stress estimation from borehole scans for prediction of excavation overbreak in brittle rock. Master's dissertation. Kingston, Ontario: Queen's University; 2017.p.270..
[74] Walton G, Kalenchuk KS, Hume CD, Diederichs MS. Borehole Breakout Analysis to Determine the In-Situ Stress State in Hard Rock. In: Proceedings of the 49th US Rock Mechanics/Geomechanics Symposium. San Francisco: American Rock Mechanics Association; 2015.p.1350-8.
[75] Papanastasiou P, Thiercelin M. Modeling borehole and perforation collapse with the capability of predicting the scale effect. Int J Geomech 2010;11 (4):286–93.
[76] van den Hoek PJ, Hertogh GMM, Kooijman AP, Kenter CJ, Papamichos E. A new concept of sand production prediction:theory and laboratory experiments. In: Proceedings of the Society of Petroleum Engineers - SPE Annual Technical Conference and Exhibition. Denver: Society of Petroleum Engineers; 1996. p.19-33.
[77] van den Hoek PJ, Smit DJ, Khodaverdian M. Material-dependent size effect of hollow cylinder stability: theory and experiment. In: Proceedings of the 1st North American Rock Mechanics Symposium, NARMS 1994. Austin: American Rock Mechanics Association; 1994.p.411-8.
[78] Papamichos E, van den Hoek PJ. Size dependency of Castlegate and Berea sandstone hollow-cylinder strength on the basis of bifurcation theory. In: Proceedings of the 35th US Symposium on Rock Mechanics, USRMS 1995. Reno: American Rock Mechanics Association; 1995.p.301-6.
[79] Lajtai EZ. Effect of tensile stress gradient on brittle fracture initiation. Int J Rock Mech Min Sci 1972;9(5):569–78.
[80] Nesetova V, Lajtai EZ. Fracture from compressive stress concentrations around elastic flaws. Int J Rock Mech Min Sci 1973;10(4):265–84.
[81] Elkadi AS, van Mier JGM. Experimental investigation of size effect in concrete fracture under multiaxial compression. Int J Fract 2006;140(1–4):55–71.
[82] Sammis CG, Ashby MF. The failure of brittle porous solids under compressive stress states. Acta Metall 1986;34(3):511–26.
[83] Lotidis MA, Nomikos PP, Sofianos AI. Numerical simulation of granite plates containing a cylindrical opening in compression. Proc Eng 2017;191:242–7.
[84] Dresen G, Stanchits S, Rybacki E. Borehole breakout evolution through acoustic emission location analysis. Int J Rock Mech Min Sci 2010;47(3):426–35.
[85] Meier T, Rybacki E, Reinicke A, Dresen G. Influence of borehole diameter on the formation of borehole breakouts in black shale. Int J Rock Mech Min Sci 2013;62:74–85.
[86] Dzik EJ, Lajtai EZ. Primary fracture propagation from circular cavities loaded in compression. Int J Fract 1996;79(1):49–64.
[87] Choens RC, Ingraham MD, Lee MY, Yoon H, Dewers TA. Acoustic emission during borehole breakout. In: Proceedings of the 52nd U.S. Rock Mechanics/ Geomechanics Symposium. Seattle: American Rock Mechanics Association; 2018.
[88] Jaeger JC, Cook NG, Zimmerman R. Fundamentals of rock mechanics. John Wiley & Sons; 2009.
[89] Carter BJ, Lajtai EZ, Yuan Y. Tensile fracture from circular cavities loaded in compression. Int J Fract 1992;57(3):221–36.
[90] Labuz JF, Shah SP, Dowding CH. Experimental analysis of crack propagation in granite. Int J Rock Mech Min Sci 1985;22(2):85–98.
[91] Ortiz M. Microcrack coalescence and macroscopic crack growth initiation in brittle solids. Int J Solids Struct 1988;24(3):231–50.
[92] Santarelli FJ, Brown ET, Maury V. Analysis of borehole stresses using pressure-dependent, linear elasticity. Int J Rock Mech Min Sci 1986;23 (6):445–9.
[93] Santarelli FJ, Brown ET. Failure of three sedimentary rocks in triaxial and hollow cylinder compression tests. Int J Rock Mech Min Sci 1989;26 (5):401–13.
[94] Bažant ZP. Size effect in blunt fracture: Concrete, rock, metal. J Eng Mech 1984;110(4):518–35.
[95] Hunt DD. The influence of confining pressure on size effect. Master's dissertation. Massachusetts Institute of Technology 1973.
[96] Bažant ZP, Xi Y. Statistical size effect in quasi-brittle structures: II. Nonlocal theory. J Eng Mech 1991;117(11):2623–40.
[97] Yavuz H, Demirdag S, Caran S. Thermal effect on the physical properties of carbonate rocks. Int J Rock Mech Min Sci 2010;47(1):94–103.
[98] Heuze FE. High-temperature mechanical, physical and Thermal properties of granitic rocks- A review. Int J Rock Mech Min Sci 1983;20(1):3–10.
[99] Keshavarz M, Pellet FL, Loret B. Damage and changes in mechanical properties of a gabbro thermally loaded up to 1000 °C. Pure Appl Geophys 2010;167 (12):1511–23.
[100] Zhang W, Sun Q, Hao S, Geng J, Lv C. Experimental study on the variation of physical and mechanical properties of rock after high temperature treatment. Appl Therm Eng 2016;98:1297–304.
[101] Kirk SS, Williamson DM. Structure and thermal properties of porous geological materials. In: Proceedings of the 17th Biennial Conference of the American Physical Society Topical Group on Shock Compression of Condensed Matter, 2011 APS SCCM. Chicago, IL; 2012.p.867-70.
[102] Abdulagatova Z, Abdulagatov IM, Emirov VN. Effect of temperature and pressure on the thermal conductivity of sandstone. Int J Rock Mech Min Sci 2009;46(6):1055–71.
[103] Ikeuchi K, Doi N, Sakagawa Y, Kamenosono H, Uchida T. High-temperature measurements in well WD-1a and the thermal structure of the Kakkonda geothermal system, Japan. Geothermics 1998;27(5-6):591–607.
[104] He MC. Application of HEMS cooling technology in deep mine heat hazard control. Mining Sci Technol (China) 2009;19(3):269–75.
[105] Yang XJ, Han QY, Pang JW, Shi XW, Hou DG, Liu C. Progress of heat-hazard treatment in deep mines. Min Sci Technol (China) 2011;21(2):295–9.